CFD as a Tool to Optimise Aeration Tank Design and Operation

Anna M. Karpinska, PhD[1] and John Bridgeman, PhD[2]

[1] Research Fellow, Department of Civil Engineering, School of Engineering, University of Birmingham, Birmingham, B15 2TT, United Kingdom. Email: annamkportela@gmail.com
[2] Professor of Environmental Engineering, Department of Civil Engineering, School of Engineering, University of Birmingham, Birmingham, B15 2TT, United Kingdom.

ABSTRACT

In a novel development on previous computational fluid dynamics (CFD) studies, the work reported here employed an Eulerian two-fluid model with the shear stress transport (SST) $k-\omega$ turbulence closure model and bubble interaction models to simulate aeration tank performance at full scale and to identify process performance issues resulting from design parameters and operating conditions. The current operating scenario was found to produce a fully developed spiral flow. Reduction of the air flow rates to the average and minimum design values led to a deterioration of the mixing conditions and formation of extended unaerated fluid regions. The influence of bubble-induced mixing on the reactor performance was further assessed via simulations of the residence time distribution (RTD) of the fluid. Internal flow recirculation ensured long contact times between the phases; however, hindered axial mixing and the presence of dead zones were also identified. Finally, two optimization schemes based on modified design and operating scenarios were evaluated. The adjustment of the air flow distribution between the control zones led to improved mixing and a 20 % improvement to the mass transfer coefficient. Upgrading the diffuser grid was found to be an expensive and ineffective solution, leading to worsening of the mixing conditions and yielding the lowest mass transfer coefficient compared to the other optimization schemes studied.

INTRODUCTION

The activated sludge (AS) process is a well documented standard for many municipal wastewater treatment plants (WWTPs) worldwide. Regardless of the site-specific process configuration, AS systems rely on a steady energy supply for operation of air compressors and recycling pumps (Karpinska Portela 2013). Aeration is the most energy-intensive unit process at municipal WWTPs and accounts for the largest fraction of the total net electricity expenditure (45-85 %) (Reardon 1995; WEF 2009). The importance of the linkage between water and energy has been recognized globally in the context of water shortages, increasing energy and material costs, climate change and food availability. To address this, the historical high energy use of aeration systems and relatively low standard oxygen transfer efficiencies of aeration devices must now be addressed via implementation of cost-effective energy management measures and engineering practices.

However, design and operation of AS systems is still largely based on empiricism, general guidelines and operator experience, often with little regard for the influence of site-specific tank hydraulics, type, number and distribution of aerators and mixers, energy input or the influence of mixing on efficient distribution of the dissolved and suspended components in the AS bioreactor (Karpinska and Bridgeman 2016; Samstag and Wicklein 2012). Numerical modelling of WWTPs has been recognized as a powerful tool, providing detailed knowledge of the unit processes, as well as reactor behaviour in response to varying input conditions. Over the last two decades the fast growth in computational power and commercialization of advanced software suites for the solution and visualization of complex flows has contributed to the successful spread of computational fluid dynamics (CFD) in wastewater engineering (Karpinska and Bridgeman 2016).

A key advantage of CFD-aided modelling of aeration tanks over the traditional and relatively well-established Activated Sludge Models (ASM) is its capacity to predict the actual flow field in multiphase non-ideal reactor systems, accounting for local scale phenomena, interfacial mass transfer and chemical reactions. A few workers have attempted to couple hydrodynamics with biokinetics to simulate the combined physical-chemical-biological processes within different AS system configurations, e.g. a full-scale oxidation ditch aerated with diffusers (Glover et al. 2006) and a lab-scale channel reactor aerated with porous tube (Le Moullec et al. 2010). While it was possible to predict simultaneously the hydrodynamics and its impact on the biochemical conversion of organics and nutrients by AS biomass, differences between concentration profiles obtained experimentally and those predicted by the numerical model were identified and reported. These errors arose from excessive model simplifications, use of a coarse grid necessitated by RAM/CPU constraints, and the need for simulation runs in realistic time frames. Consequently, the coupled CFD-ASM simulation of AS tanks remains a challenge, due to the complexity of the models involved and the solution accuracy which demands a high level of mesh refinement resulting in significant computational requirements and long run times (Karpinska and Bridgeman 2016). Therefore, common practice is to simplify the modelling approach in a computationally efficient manner, to simulate individual components of the AS system separately, and to couple the results afterwards (Pereira et al. 2012). The literature offers several examples of the use CFD to study aeration process in different AS systems, e.g. to acquire an insight into the mutual interaction between the phases and the global and local mass transfer coefficients (Cockx et al. 2001; Fayolle et al. 2007), to assess the impact of the diffuser arrangement on mixing patterns and nitrification (Gresch et al. 2011) and to identify operating scenarios that promote the formation of anoxic zones reducing energy expenditure on aeration (Yang et al. 2011).

To date, no agreed protocol for robust CFD modelling of aeration tanks has been defined. Nonetheless, the modelling procedure exploiting the most computationally inexpensive modelling scenario, based on the Reynolds-Averaged Navier-Stokes (RANS) equations closed by the standard $k-\varepsilon$ model, a neutral density Eulerian model, and constant bubble size assumption has become widely accepted by the wastewater modelling community as a standard approach (Karpinska and Bridgeman 2016; Samstag et al. 2016). However, the pitfalls of that modelling scheme have been reflected in overestimated values of the volumetric mass transfer coefficient $k_L a$ (Fayolle et al. 2007; Le Moullec et al. 2010). Nonetheless, the proposed method to rectify this error focused exclusively on determination of the actual bubble sizes either experimentally or through implementation of add-on statistical models. This underestimated the influence of the dispersed model on predicted values of turbulent kinetic energy dissipation rate ε, involved in computation of the mass transfer coefficient, $k_L a$, and hence the simulations of dissolved oxygen (DO) and organics and nutrients transformations in the AS process (Karpinska and Bridgeman 2017).

Unlike most previous CFD models of aeration systems, the work reported here used the SST $k-\omega$ turbulence model (Menter 1994) to account for the turbulent interactions between the gas and liquid phases to analyse the performance of a full-scale conventional plug flow AS tank aerated and mixed by means of fine pore diffusers. Moreover, the dynamic changes in bubble sizes due breakage and coalescence were simulated using the Hibiki-Ishii model (Hibiki and Ishii 2000) embedded into the transport equation for interfacial area concentration (IAC). The selection of this modelling approach, developed previously for the lab-scale aeration tanks (Karpinska and Bridgeman 2017) was justified by its reliability in prediction of the turbulent interactions between the phases and resulting oxygen transfer, outperforming the standard $k-\varepsilon$ model. The impact of the design and operating parameters on the flow field induced by the aeration system and the resulting gas holdup were assessed to detect and quantify the shortcomings of each operating scenario. Simulations of the RTD of the fluid in the AS tank were performed to determine the influence of the current operating conditions on the macromixing and reactor performance and to quantify site-specific process limitations. Finally, two optimization scenarios based on the modification of either operating parameters or diffuser density were evaluated taking into consideration mixing and oxygen mass transfer in the tank.

METHODS

Full-scale Aeration Tank

WWTP 'A', located in the Midlands region of the UK serves a population equivalent of 450000 and treats an average 120000 m^3 of wastewater each day. Biological treatment consists of three AS modules, each having four identical, rectangular plug flow tanks aerated by means of fine pore diffusers. The single AS tank has an active volume of approximately 5000 m^3 and consists of anoxic and aerated compartments separated by a baffle (Fig. 1a). The anoxic zone constitutes 11 % of the total tank volume. The average influent flow rate into the single tank is 10800 $m^3\ d^{-1}$ (max. 20000 $m^3\ d^{-1}$), and the Return Activated Sludge (RAS) flow rate is 6750 $m^3\ d^{-1}$ (max. 12500 $m^3\ d^{-1}$). The tank is equipped with 1920 dome diffusers fixed over the tank bottom in a full-floor coverage configuration (Fig. 1b). The aeration system is divided into two control zones, Z1 and Z2 (Fig. 1c), with differing diffuser density and operating air flow rates. The airflow distribution between Z1 and Z2 is 60 and 40 %, respectively. The process design parameters characterizing aeration system are listed in Table 1. For convenience, the parameters enabled in optimization studies are also included in the table. Currently, the AS tanks are operated at the average influent and maximum design air flow rate. The target DO concentration in both zones is 2.0 mg L^{-1}.

Numerical Studies - CFD

3D geometry and mesh

The three-dimensional (3D) geometry of the aeration tank was designed using ANSYS 17.0 Design Modeler pre-processor. The work presented here considered only the aeration tank compartment, hence the anoxic zone was not included in the computational domain. The grid was generated using sweep and patch conforming methods and the face sizing function was used to refine the mesh in the diffuser regions (Supplementary Information, Fig. S1). Three meshes, comprising 1.2 to 3.8 million hexa- and tetrahedral cells were produced initially (Table 2).

The Grid Convergence Index (GCI) approach (Roache 1998) was employed in grid refinement studies as a recommended uncertainty estimator method. The outcomes of the GCI calculations and the grid independence studies are provided in Supplementary Information (Table S1 and Figs. S2-S3, respectively). The results indicated that mesh 2, having 2.2 million elements, was appropriate for the subsequent modelling work.

Modelling approach

Simulations of the hydrodynamics, mass transfer and macromixing in the lab-scale aeration tank were performed using ANSYS 17.0 Fluent CFD software. Each simulation was run in parallel on the University of Birmingham BlueBEAR Linux HPC Cluster using dual-processor 8-core (16 cores/node) 64-bit 2.2 GHz Intel Sandy Bridge E5-2660 worker node with 32 GB of RAM.

Hydrodynamics

The multiphase flow in AS tank was simulated with an Eulerian two-fluid model derived from unsteady RANS (URANS) equations and the two-equation SST $k-\omega$ turbulence model, following Karpinska and Bridgeman (2017). The governing equations representing conservation of mass and momentum for each phase, described comprehensively in Karpinska and Bridgeman (2016) and the bubbly flow models, can be found in Supplementary Information.

Mass transfer

The aeration process was reproduced numerically via a species mass transfer model. Oxygen was treated as an active scalar and the effects of its gradients across the domain were coupled to the momentum equation. Two scalars representing transport of concentration in the primary and secondary phase can be written in general form following Talvy et al. (2007):

$$\frac{\partial \alpha_{ph} c_{ph}}{\partial t} + \vec{\nabla}\left(\alpha_{ph} c_{ph} \vec{v}_{ph}\right) = -\vec{\nabla}\left(\alpha_{ph}\left(\vec{J}_{ph} + \overline{c'_{ph} v'_{ph}}\right)\right) + \overline{c_{ph} m_{ph}} + \overline{L_{ph}} \tag{1}$$

where α_{ph} is volume fraction of liquid/gas phase, c_{ph} is local instantaneous scalar concentration in phase, t denotes time, $\vec{J}_{ph}$ is the flux due to molecular diffusion, the term $\overline{c'_{ph} v'_{ph}}$ denotes turbulent diffusion of the concentration, $\overline{c_{ph} m_{ph}}$ represents the transport of concentration c_{ph} by mass transfer and L_{ph} is interfacial transfer of concentration between the phases.

The interfacial oxygen mass transfer occurring between air bubbles and liquid phase can be written as (Talvy et al. 2007):

$$\overline{L_{ph}} = \overline{L_L} = k_L a(C_L^* - C_L) \tag{2}$$

where L_L is interfacial mass transfer between air bubble and liquid, k_L is the local mass transfer coefficient, a is the interfacial area, C_L^* is oxygen saturation concentration, C_L is actual oxygen concentration and the term $(C_L^* - C_L)$ is the driving force causing oxygen transfer.

The local mass transfer coefficient k_L is obtained from the Higbie penetration theory (Higbie 1935):

$$k_L = 2\sqrt{\frac{D_L v_r}{\pi d_b}} \tag{3}$$

where D_L is molecular diffusion coefficient of oxygen in water at 20°C, v_r is relative velocity between the phases and d_b is bubble diameter.

The interfacial area a is calculated as (Fayolle et al. 2007):

$$a = \frac{6}{d_b}\frac{\alpha_G}{1-\alpha_G} \tag{4}$$

where α_G denotes volume fraction of air phase.

In the work reported here, the global volumetric mass transfer coefficient $k_L a$ was implemented via a User Defined Function (UDF) routine written in C language. Successively, the α factor, being a factor applied to the mass transfer coefficient to account for substrate and nutrient loading variations within the reactor, was used to modify (i.e. reduce) the CFD-derived $k_L a$ in standard conditions (= $k_L a_{20}$) in order to account for the effects of shrinking gas-liquid interface surface area due to surfactant accumulation on the bubble and mean cell residence time. Considering a plug flow AS system characterized by varying substrate loading along the tank, the recommended values of 0.3< α<0.8 (WPCF-ASCE 1988) were applied to represent oxygen transfer rates in process conditions ($\alpha k_L a_{20}$) in both control zones.

Macromixing

The overall mixing in the aeration tank was studied numerically through the simulation of a pulse tracer experiment. The RTD of the fluid (Danckwerts 1953) was computed from the time history of a tracer concentration recorded at the outlet of the aeration tank. The transport of the nonreactive tracer injected into the fluid entering the tank at the inlet was modelled using a passive scalar approach, based on prediction of the local mass fraction of tracer species, Y_{tr}. Assuming no tracer production in the system, its transport due to convection and diffusion can be written in the general form as (Glover et al. 2000):

$$\frac{\partial}{\partial t}(\rho_L Y_{tr}) + \nabla(\rho_L \vec{v}_L Y_{tr}) = -\nabla \vec{J}_{tr} + S_{tr} \tag{5}$$

where ρ_L denotes density of the liquid, $\vec{v}_L$ is velocity of the liquid phase, $\vec{J}_{tr}$ is diffusive mass flux of tracer; and S_{tr} is the source term which injects tracer into the domain by addition any user-defined sources.

The RTDs of the fluid expressed as normalized exit age distribution function $E(t)$ is defined as (Fogler 1999; Levenspiel 1999):

$$E(t) = \frac{Q_e C(t)}{M} \tag{6}$$

where Q_e is the effluent flow rate, M is the quantity of the introduced tracer and $C(t)$ denotes concentration-time series recorded in the outflow from the tank.

The observed mean residence time τ is (Levenspiel 1999):

$$\tau = \frac{\int_0^\infty tC\ dt}{\int_0^\infty C\ dt} \cong \frac{\sum_i t_i\, C_i \Delta t_i}{\sum_i C_i \Delta t_i} = \frac{V}{Q_e} \tag{7}$$

where V denotes the reactor volume.

Additional modelling details can be found in Supplementary Information.

Model setup, boundary and operating conditions

The properties of the primary and secondary phases are summarized in Table 3. The modelling of hydrodynamics and mass transfer in the aeration tank was achieved by setting water and air as a working fluid. A parallel modelling scenario based on the passive scalar approach was run, in which the continuous phase was defined as a mixture of water and AS. RTD simulations considered a tracer having physical properties equal to those of water. The boundary and operating conditions were summarized in Table 4.

Convergence criteria for the solutions were set at 10^{-6}. For the sake of stability of convergence of the SST $k - \omega$ model, the first 10^5 iterations were run with an initial time step size (Δt) of 0.001 s. With stable residual monitors, Δt was gradually increased to 0.1 s.

All the hydrodynamic simulations considered a flow time equivalent to 24 h (≈2.5 times greater than the designed hydraulic retention time, τ= 9.6 h). The RTD simulations considered a flow time of 50 h.

Experimental Studies

Measurement of the liquid-phase velocity

The 3D velocity of the mixed liquor was measured using an acoustic Doppler velocimeter (ADV) (Nortek AS, model Vectrino Plus), operating at acoustic frequency of 10 MHz, sampling rate of 200 Hz and with 7 mm vertical extent of the sampling volume. The measurements were performed from a platform located above Z2 and at a distance (L) of 30.0 m from the outflow weir. Location of the measurement points was dictated by access and power restrictions. The velocity was measured in 10 points distributed across the lane at two depths (y), 0.3 and 0.7 m below the surface. The ADV sensor was attached to a custom-made aluminium structure fixed to the handrail to render it immobile. During measurements, a total of 40000 velocity data points were collected at each measurement location. In order to remove invalid data noise (related to the presence of the dispersed air bubbles moving with different velocities than the liquid phase and, to a lesser extent, due to Doppler signal aliasing (Mori et al. 2007)), the output ADV velocity time-series were processed by Velocity Signal Analyser (VSA) software (Jesson et al. 2015) using a correlation and signal-to-noise-ratio (SNR) pre-filter, Modified Phase-Space Thresholding (PST) despiking filter and linear interpolation method of spike replacement. The ADV data-cleaning procedure is discussed in detail in Karpinska and Bridgeman (2017).

Mixed liquor analysis

Composition of the mixed liquor in the AS tank was evaluated from the results of measurements of DO and Mixed Liquor Suspended Solids (MLSS) and the analyses of the

Biochemical Oxygen Demand (BOD), ammonia nitrogen (NH_4-N), and nitrates (NO_3-N) concentrations in samples taken from ten points distributed along the aeration tank. Access limitations meant that location of the measurement points was restricted to 0.4 m from the external wall. MLSS concentrations were measured in 36 points within the same vertical cross-section over Z2 as the liquid velocity. MLSS and DO concentrations were measured directly with optical sensors (Hach HQ40 IntelliCal LDO101 Field Luminescent DO probe and Partech 740 Monitor) fixed to a submerged telescopic support. In order to determine longitudinal concentration profiles, DO and MLSS concentrations were measured at each sampling point at three depths: *viz*. 0.1 m below the fluid surface; at mid-depth (2.60 m); and just above the diffusers, at 5.0 m. BOD and nutrients were determined indirectly from analyses of the mixed liquor samples pumped carefully from the same three depths from the sampling points. 50 mL aliquots were transferred to labelled plastic containers and transported to the laboratory for immediate colorimetric assays using a Hach DR/890 Portable Colorimeter and Hach Test'N Tube Vial kits: AmVer™ Salicylate Method and NitraVer™ X Chromotropic Acid Method. BOD was determined in accordance with Luminescence Measurement of DO in Water and Wastewater using Hach HQ40 IntelliCal BOD LDO.

RESULTS AND DISCUSSION

Concentration Patterns in a Full-scale AS Tank

Preliminary experiments were performed to gain an insight into the site-specific aeration process performance. Fig. 2 illustrates the DO, BOD and nutrients concentration profiles along the full-scale AS tank. Relatively minor DO concentration gradients were observed over the depth in the majority of the measurement points in Fig. 2a. These are likely to be an effect of the rising bubbles from the diffusers promoting vertical mixing. DO levels measured from the anoxic tank along the first 50 m were low (0.3 - 1.0 mg L^{-1}). Thereafter, DO concentrations rose in an approximately linear manner for 50 m to a maximum DO concentration of 3.1 mg L^{-1}, whereupon they decreased, again linearly, to 1.1 mg L^{-1} at the outlet. At the same time, the readings from the WWTP's online LDO analysers (Hach Lange sc100) for sensors located in the middle of the lane at depth of 1.0 m were: 0.35 mg L^{-1} in Z1; and 3.08 mg L^{-1} in Z2, compared to the set-point values of 2.0 mg L^{-1}. During several visits to the WWTP, the same trend of non-equal DO concentrations in both zones was observed. Oxygen transfer rates in the AS tank are governed by the local hydrodynamics; hence the variations in DO concentration are a function of the hydrodynamic time-scales (in seconds). For this reason, thorough analysis of the specific DO patterns in Fig. 2a requires assessment of the overall mixing phenomena, accounting for the site-specific process conditions, such as diffusers age and performance and wastewater temperature. At the same time, BOD and nutrients concentrations are governed by biokinetic time-scales (sludge age) measured in days. Hence, the concentration profiles shown in Figs.2 b-d mirror the longer-term effects of the adopted aeration scenario rather than response to the actual oxygenation rates. Accordingly, while there is no clear pattern in vertical distribution of the concentrations, the biokinetic-related parameters shown all correlate with each other as expected.

Similar to DO, the MLSS distribution within the tank is closely related to the local hydrodynamics. The longitudinal evolution of the MLSS profile is shown in Figure 3a. The solids content along the length of the tank ranged from 3160 to 3420 mg L^{-1}. MLSS sensor readings at three depths within the same sampling point differed by less than 5 %. Fig. 3b shows the transverse MLSS profile through Z2. The MLSS concentration measured in 36 points was found to vary from 3280 to 3360 mg L^{-1} (a difference of 2.4 %), indicating approximately homogenous distribution of the solids in the section analysed. The approximately uniform solids content (Figs. 3a-b), and the lack of evident settling zones associated with locally increased MLSS values, are a result of the favorable mixing conditions achieved at the given operating air flow rate.

Validation of the CFD Model

Preliminary numerical studies considered two different simulation schemes for prediction of the flow field in the aeration tank. The results of the simulations performed for water-air and water-air-sludge scenarios subject to the same operating air and influent flow rates (Q_a and Q_L) yielded similar velocity contour maps and distribution of the velocity vectors (Supplementary Information, Fig. S4) and hence the less computationally expensive neutral density simulations were found to be suitable to represent liquid flow patterns within the AS tank.

To validate the CFD model used in prediction of the air-induced mixing of the liquid phase, despiked ADV data points representing average velocity magnitude were plotted against CFD results corresponding to the measurement points across zone Z2 (Fig. 4). The figures illustrating raw and despiked velocity-time series and the resulting velocity magnitude are provided as Supplementary Information (Figs. S5-S7). The CFD simulations were performed considering actual operating conditions in the AS tank, *viz.* the average influent flow rate (Q_L= 0.1 m^3 s^{-1}) and the maximum air flow rate (Q_a= 1.1 m^3 s^{-1}). The average liquid velocity magnitude in the analysed cross-section measured at depths of 0.3 and 0.7 m varied from 0.12 to 0.22 m s^{-1} and from 0.15 to 0.18 m s^{-1}, respectively. When comparing the numerical and experimental results shown in Fig. 4 it is evident that the CFD model reproduced the values of the local velocities at measurement points located at L = 0.4, 1.9 and 3.3 m (y = 0.3 m) and L = 0.4, 3.3 and 6.3 m (y = 0.7 m), respectively with good accuracy. The liquid velocities at L = 6.3 m (y = 0.3 m) and 1.9 m (y = 0.7 m), although slightly overestimated by the numerical model, were still in good agreement with the experimental data. However, at L = 4.8 m from the internal wall, the CFD model overestimated the velocities at both depths. One reason for the difference between the measurement and simulation results may be that the SST $k - \omega$ model is based on the Bussinesq isotropic eddy viscosity assumption, which may lead to inaccurate prediction of the flows driven by anisotropy of the normal Reynolds stresses and secondary shear stresses, and flows characterized by large extra strains (Bridgeman et al. 2008). Alternatively, the discrepancy may be a result of poor aerator performance, likely due to the device ageing, fouling and scaling. While CFD simulations did account for the uniform flow distribution to each diffuser and non-uniform inlet bubble sizes to approximate changes in diffuser porosity over time, the possibility of faulty performance of partially or entirely clogged diffusers below the ADV sensor was not considered. Nonetheless, good agreement between the numerical and experimental data in 8 of 10 measurement points provides confidence that the CFD model was able to predict the hydrodynamics of the full-scale aeration tank.

Impact of the Operating Conditions on the Hydrodynamics in AS Tank

Figs. 5 and 6 show the liquid and air velocity magnitude and air holdup in the aeration tank for different operating conditions. In Fig. 5, the vector and contour maps on the left side represent vertical cross-sections through zones Z1 and Z2 at $L = 30.0$ m, while the contour maps on the right side (with flow direction indicated by an arrow), relate to the horizontal cross-section through the mid-depth ($y = 2.6$ m).

Gas holdup is a key hydrodynamic parameter governing distribution of the interfacial surface area between the air and liquid phases. Thus, for the given diffused air system, selection of the optimal operating conditions yielding higher air holdups is essential to achieve oxygen transfer rates required by the AS process. Fig. 6 shows that the spatial distribution of the gas holdup in the analysed sections follows the pattern observed in air velocity profiles. Slightly higher air velocities and volume fractions observed in zone Z1 result from the more dense arrangement of the diffusers in comparison with zone Z2. Flow regions characterized by the highest air velocities are usually associated with either presence of larger bubbles, including those generated in coalescence-inducing turbulent flow conditions, or with the co-current flow of both phases. Low-air velocity regions are associated with counter-current movement of swarms of minute bubbles having larger interfacial surface areas, a proportion of which may have been generated due to impact with turbulent eddies.

Figs. 5a-6a show the CFD results obtained for the actual operating conditions at the WWTP. The current aeration scenario results in fully developed spiral flow, characterized by liquid loop circulation with limited mixing in the axial direction. The smallest fluid velocities occur in the centre of the rotating cells and in the bend of the tank, as seen in the horizontal velocity profile (Fig. 5a). The decrease in air holdup observed in Z2 (Fig. 6a) is likely to be due to the larger intervals between the diffuser rows (Fig. 1c). This operating scenario resulted in some aeration of the central portion of the tank, as shown by the higher values of air volume fractions (up to 0.6 %), whereas adjacent to the lateral walls and above the tank bottom, the air holdup decreases to zero, possibly linked to the occurrence of the locally lower DO concentrations.

Similar spiral flow patterns were observed for the average operating air flow rate of 0.7 $m^3\ s^{-1}$ (Fig. 5c); however, a decrease of the liquid velocities and smoothed flow patterns in the horizontal section through the tank were also observed. Furthermore, a significant decrease in values of the gas holdup in the tank to around 0.3 % was also observed (Fig. 6c), giving rise to lower oxygenation capacities imposed by this operating mode.

Doubling the influent flow rate to the maximum design value Q_L of 0.2 $m^3\ s^{-1}$ resulted in the formation of two circulating counter-current flow loops observed in the section through Z1 (Fig. 5b). This flow pattern was observed to destabilize over the length of the reactor, resulting in re-occurrence of the single rotating cell in Z2. The influence of the air velocity shown in Fig. 6b on the liquid flow field is also evident. At the same time, the increase of the liquid velocities yielded an improved distribution of the gas holdup in Z2 compared to the current operating scenario (Fig. 6a).

The lowest air flow rate of 0.5 $m^3 s^{-1}$ yielded the poorest air mixing scenario in terms of increased percentage of the tank regions where fluid velocity was found to drop below 0.1 m s^{-1} (Fig. 5d), giving rise to possible sludge settling. The change of the $Q_L : Q_a$ ratio led to formation of two counter-current rotating cells along the whole tank. Nonetheless, this operating air flow rate was insufficient to aerate the tank contents sufficiently (Fig. 6d), yielding the lowest air holdup of around 0.1 %.

Considering the results of the simulations performed for all aeration process design parameters, the choice of the current operating scenario for the average Q_L ensuring highest air holdups is justified. Therefore, the subsequent studies reported below focus on further characterization of the mixing patterns within the tank induced by the diffusers operated at maximum air flow rate.

Residence Time Distribution

The RTD of the fluid in the AS tank was calculated to evaluate the impact of the flow patterns induced by the site-specific aeration system on the macromixing and the reactor performance. Evolution of the $E(t)$ curve shown in Fig. 7 corresponds to the typical output curve of n-CSTRs (Continuous Stirred Tank Reactors) in series. The observed mean residence time τ (vertical dashed line) was 8.3 h, 14 % shorter than the design value of 9.6 h. The analysis of the area below the $E(t)$ curve showed that by time $t = \tau$, 60% of the injected tracer had exited the AS tank, whilst its complete removal from the system took place after 40 h (=4.8 τ). It is believed, that the prolonged contact time between the phases (indicated by $t > \tau$) is likely to have been caused by the internal recirculating eddies in the vertical direction, usually associated with flow patterns of the rising bubbles and the spiral flow (Fig. 5a). On the other hand, a characteristic shallow tail in the $E(t)$ curve (Fig. 7) indicates the presence of stagnant fluid regions, and consequently, reduction of the active volume of the tank available for biochemical processes. This outcome is also consistent with the conclusions drawn from the analysis of the liquid phase velocities in Fig. 5a. Retention of the remainder of the tracer in dead volumes and its hindered transport in the axial direction is manifested through its delayed washout from the system, yielding a long RTD tail. Thus, it is clear that the spiral flow contributes to the extension of the mixing time, whereas hindered longitudinal mixing and occurrence of the stagnant fluid regions may have an adverse effect on the oxygen transfer and biochemical conversion reaction rates, and therefore on the efficiency of the treatment processes, and on nitrification in particular.

Improvements to Mixing Patterns in the AS Tank

Two scenarios for improving mixing, and hence process performance, in the aeration tank were considered; *viz.* (i) alteration of the operating parameters, and (ii) modification of the diffuser grid through addition of one unit to each row (Fig. S7), whilst maintaining original operating influent and air flow rates (Table 1).

The power required for blower operation was estimated using the adiabatic compression equation (Mueller et al. 2002; Tchobanoglous et al. 2003):

$$P = \frac{w\mathrm{R}T}{29.7 \cdot 0.283 \cdot e_B \cdot e_M}\left[\left(\frac{p_{out}}{p_{in}}\right)^{0.283} - 1\right] \quad (8)$$

where P is the power requirement for each blower, w is air mass flow rate, R is universal gas constant for air (R= 8.314 kJ kmol^{-1}K^{-1}), T is the design inlet temperature, p_{in} and p_{out} are absolute pressures at the inlet assumed atmospheric and outlet assumed 2.0 atm (following Quasim (1999)) of compressor , e_B and e_M are blower and motor efficiencies.

Assuming typical values of e_B and e_M (70 % and 92 %) the compressor power demand (Eq. 8) was found to be 130 kW.

For scenario (i), the flow distribution in the control zones Z1 and Z2 was adjusted from 60 % and 40 % to 75 % and 25 % in an attempt to destabilize the spiral flow and to improve aeration (higher air holdup) in zone Z1. The reduction of the air flow rate in zone Z2 aimed to ensure more uniform distribution of the air bubbles within the tank volume, as observed in the contour map of gas holdup in Fig. 6c.

The results of the CFD analyses were compared with the original design and operating scheme, as shown in Fig. 8. Liquid and air velocities and gas holdup values are summarized in Table 5. The operational changes resulted in an increase of the liquid velocity in the centre of Z1 (Fig. 8b), reducing stagnant regions adjacent to the lateral walls and in the centre of the rotating cell (Fig. 8a). However, the features of the fluid circulation loops found in the original design were still preserved, especially in Z2. The average liquid velocity of 0.25 m s^{-1} in cross-section Z1 was lower than in the case of the original scenario (Table 5), in contrast to the horizontal section, where the new scheme yielded slightly higher fluid velocities of 0.23 m s^{-1}. As expected, the induced gas holdup was more uniformly distributed within both zones and yielded significantly higher values up to 0.6 % in section through Z1 in comparison with the original operating scheme, but distinctly lower in Z2 (0.2 %).

In line with expectations, the air flow split between the larger number of diffusers led to a reduction of the air velocities in the control zones in comparison with the original design (Fig. 8c). Diffused air is the main driving force inducing fluid motion in the tank, and therefore the modified layout resulted in a 50 % decrease of the average axial liquid velocities to 0.11 m s^{-1} (Table 5). The lack of spiral flow loops observed in the original scenario and less intense vertical mixing manifested by lower fluid velocities were also seen in the vertical section through the tank (Fig. 8c). Such flow conditions promoted longer contact times between the phases providing the most homogenous aeration in both control zones in comparison with other operation scenarios investigated. The air holdup of 0.5 % in Z1 (Table 5) was also higher than the one resulting from the original diffusers arrangement.

Oxygen Transfer in the AS Tank

The oxygen transfer rate in aeration tanks is governed by several hydrodynamic parameters, *viz.* bubble size, velocity and turbulence in the liquid phase and resulting gas holdup (Karpinska and Bridgeman 2017). Accordingly, higher values of liquid velocities, ε and air holdup were observed for all operating and design scenarios in zone Z1, resulting in distinctly higher global mass transfer coefficients than in zone Z2, as seen when comparing data summarized in Table 5. The maximum value of $k_L a_{20}$ of 224 d^{-1} in Z1 was reported for the scheme based on an adjustment to the air flow distribution. The air holdup in Z2 was the lowest, yielding a value of $k_L a_{20}$ nearly three-times lower than the original scenario. The operating scheme with an increased number of diffusers was found to yield relatively high air holdups in both zones, but distinctly lower liquid velocities and hence, ε (Table 5). For this reason, the resulting oxygen transfer rate coefficients were lower than the ones obtained with the original design scenario. After the simulated aeration time of 15 mins, a constant equilibrium DO concentration was achieved for all three operating scenarios, which was in the range of 10.1-10.3 mg L^{-1} in both control zones (Table 5). Due to the different global values of $k_L a_{20}$ in control zones, the equilibrium DO concentration in Z1 was achieved in a much shorter time than in Z2 (3.7 mins for the original design, 2.2 mins for modified operating scenario and 5.2 mins for modified design). Similar observations were identified for the operating scenario with adjusted distribution of the air flow between the control zones. In this case, improvement of the horizontal mixing and the highest mass transfer rates resulted in markedly faster and uniform oxygenation of zone Z1, whereas the decrease of $k_L a_{20}$ in Z2 contributed to a longer aeration time being required to achieve saturation DO concentration. At the same time, modification of the diffuser density resulted in lower oxygenation rates, requiring longer contact times to achieve DO equilibrium levels, but characterized by a more homogenous evolution of the DO profile across the AS tank. The DO profiles along and across the tank are provided in Supplementary Information (Figs. S8a-c)

Discussion

Analysis of the CFD results shows that adjustment of the air flow rate distribution between the control zones resulted in the highest oxygen transfer rate in zone Z1, which is subject to the highest (influent) BOD and ammonia loadings. Since the oxygen uptake by biomass decreases over the length of the plug flow tank, further reduction of the oxygen transfer rates in zone Z2 resulting from the imposed scenario should not affect overall aerobic process efficiencies. However, this assumption requires further investigation through e.g. experimental assessment of the oxygen transfer and biochemical reaction rates. At the same time, the scenario based on the increase of diffuser density results in moderate oxygenation rates in Z1, but a doubling of oxygen transfer rates in Z2 compared to the original design. Nonetheless, this setup requires capital costs associated with the diffuser grid upgrade. The recommended α values for plug flow tanks were used to reduce the global $k_L a_{20}$, in order to represent mass transfer coefficient values in control zones Z1 and Z2 having different oxygen uptake rates due to non-uniform substrate and nutrient loading along the tank. Assuming that the DO profile observed in Fig. 2a was representative of the simulated original operating scenario (over-aeration of the zone Z2) and comparing the data listed in Table 5, modification of the diffuser layout and consequential lowering of $\alpha k_L a_{20}$ in Z1 from 56 to 48 d^{-1} can be seen to result in insufficient aeration performance to satisfy biodegradation and nitrification oxygen requirements. In this context, modification of the process parameters is the only viable among the analysed scenarios, to ensure the high oxygen transfer conditions necessary to boost biochemical conversion reactions rates. In this case, the $\alpha k_L a_{20}$ in Z1 was the highest (67 d^{-1}), exceeding the value obtained for the original design by almost 20 %.

CONCLUSIONS

The research presented in this paper evaluated and then improved performance of a full-scale plug flow aeration tank through CFD simulations of hydrodynamics, macromixing and mass transfer. The following key conclusions have been drawn:

- A validated CFD approach based on the SST $k-\omega$ turbulence closure model and the IAC model was used to assess the hydrodynamics of a full-scale AS tank. The results were used to identify and localize adverse phenomena resulting from the imposed operating conditions. The maximum operating air flow rate resulted in formation of spiral flow conditions. Increasing the influent flow to the maximum design value improved mixing and aeration of the fluid volume. The results obtained with average and minimum design air flow rates gave rise to the formation of extended unaerated fluid volumes associated with the stagnant fluid regions, possible sludge settling and limited distribution of the bubble plume.
- Macromixing data were used to assess the impact of air-driven mixing on reactor behaviour and quantification of the site-specific process limitations. Internal recirculation of the flow, linked to rising bubbles promoted extended contact times between the phases, ensuring efficient oxygenation of the fluid. However, hindered axial mixing and the presence of the dead zones reducing the active volume of the AS tank are suspected to have a significant impact on the oxygen transfer and the reaction yield, and thus the treatment process performance.
- Considering the optimization scenarios investigated, adjustment of the air flow distribution between the control zones led to improved mixing and reduction of the dead volumes, and furthermore yielded the highest $\alpha k_L a_{20}$ of 67 d^{-1} in Z1 outperforming the original design scenario by 20 %. The more capital intensive optimization scenario related to upgrade of the diffuser grid provided a more uniform

aeration pattern. However, the resultant significant decrease of the fluid velocities gave rise to the lowest $\alpha k_L a_{20}$ of 48 d^{-1} compared with the other scenarios. In this context, modification of the process parameters would appear to be the only feasible solution to ensure high oxygen transfer rates in the influent zone which is subject to highest BOD and ammonia loadings.

- The CFD analysis presented in this work, validated using hydrodynamic-, macromixing- and mass transfer data, demonstrates the technique’s use for prediction of reactor behaviour and process performance at varying operating conditions, as well as troubleshooting and optimization, and provides a blueprint for future workers in the field.
- The follow-up study will focus on improved experimental characterization of the reactor performance, expanded through the determination of the oxygen uptake- and biochemical reaction rates and the RTDs.

ACKNOWLEDGEMENTS

The research work of Dr. Anna M. Karpinska Portela was funded by the College of Engineering and Physical Sciences, University of Birmingham, UK.

NOMENCLATURE

The following symbols are used in this paper:

$a =$ interfacial area;

$C =$ concentration;

$C_L =$ bulk liquid phase oxygen concentration;

$C_L^* =$ oxygen saturation concentration in a liquid phase;

$c_{ph} =$ local instantaneous scalar concentration in phase;

$c'_{ph} =$ local instantaneous concentration in phase;

D_h = hydraulic diameter;

D_L = liquid molecular diffusivity;

d_b = bubble diameter;

I = turbulence intensity;

$\vec{J}_{ph}$ = flux due to molecular diffusion;

$\vec{J}_{tr}$ = flux of tracer due to molecular diffusion;

k = turbulent kinetic energy;

k_L = local mass transfer coefficient;

$k_L a$ = volumetric mass transfer coefficient;

$k_L a_{20}$ = clean water volumetric mass transfer coefficient at 20°C;

L = distance;

L_L = interfacial mass transfer;

L_{ph} = interfacial mass transfer between the phases;

M = quantity of tracer;

m_{ph} = local instantaneous interfacial mass transfer;

P = power;

p = pressure;

p_{in} = inlet blower pressure;

p_{out} = outlet blower pressure;

Q_a = air flow rate;

Q_e = effluent flow rate;

Q_L = influent flow rate;

S_{tr} = source term representing rate of creation of tracer from and any user-defined sources;

T = temperature;

t = time;

V = volume;

$\vec{v}_{dr}$ = drift velocity;

$\vec{v}_G$ = velocity of gas phase;

$\vec{v}_i$ = interfacial velocity;

$\vec{v}_L$ = velocity of liquid phase;

$v_{L,hor}$ = velocity of liquid phase in a horizontal section through the tank;

v'_{ph} = local instantaneous velocity;

$\vec{v}_{ph}$ = phasic velocity;

v_r = relative velocity;

w = air mass flow rate;

Y_{tr} = mass fraction of the tracer;

y = depth;

α = factor applied to the mass transfer coefficient to account for substrate and nutrient loading variations within the reactor, (i.e. ratio of process- to clean- water $k_L a$);

α_G = volume fraction of gas;

α_L = volume fraction of liquid;

α_{ph} = phasic volume fraction;

α_{tr} = volume fraction of tracer;

ε = turbulent kinetic energy dissipation rate;

μ_L = dynamic viscosity of the liquid phase;

ρ = density;

ρ_G = density of the gas phase;

ρ_L = density of the liquid phase;

τ = mean residence time; and

ω = specific turbulence dissipation.

SUPPLEMENTAL DATA

The GCI calculations, governing equations related to hydrodynamics and IAC model, Table S1 and Figs. S1-S9 are available online in the ASCE Library (ascelibrary.org)

REFERENCES

Bokil, S. D., and Bewtra, J. K. (1972). "Influence of mechanical blending on aerobic digestion of waste activated sludge." *Proc., 6th Int. Association on Water Pollution Research and Control (IAWPRC)* Jerusalem, 421-438.

Bridgeman, J., Jefferson, B., and Parsons, S. (2008). "Assessing floc strength using CFD to improve organics removal." *Chem. Eng. Res. Des.*, 86(8), 941-950.

Cockx, A., Do-Quang, Z., Audic, J. M., Liné, A., and Roustan, M. (2001). "Global and local mass transfer coefficients in waste water treatment process by computational fluid dynamics." *Chem. Eng. Process.*, 40(2), 187-194.

Danckwerts, P. V. (1953). "Continuous flow systems. Distribution of residence times." *Chem. Eng. Sci.*, 2(1), 1-13.

Fayolle, Y., Cockx, A., Gillot, S., Roustan, M., and Héduit, A. (2007). "Oxygen transfer prediction in aeration tanks using CFD." *Chem. Eng. Sci.*, 62(24), 7163-7171.

Fogler, H. S. (1999). *Elements of chemical reaction engineering*, Prentice-Hall International, London.

Glover, G. C., Generalis, S. C., and Thomas, N. H. (2000). "CFD and bubble column reactors: simulation and experiment." *Chem. Pap. - Chem. Zvesti*, 54(6A), 361-369.

Glover, G. C., Printemps, C., Essemiani, K., and Meinhold, J. (2006). "Modelling of wastewater treatment plants - how far shall we go with sophisticated modelling tools?" *Water Sci. Technol.*, 53(3), 79-89.

Gresch, M., Armbruster, M., Braun, D., and Gujer, W. (2011). "Effects of aeration patterns on the flow field in wastewater aeration tanks." *Wat. Res.*, 45(2), 810-818.

Hibiki, T., and Ishii, M. (2000). "One-group interfacial area transport of bubbly flows in vertical round tubes." *Int. J. Heat Mass Tran.*, 43(15), 2711-2726.

Higbie, R. (1935). "The Rate of Absorption of a Pure Gas into a Still Liquid during Short Periods of Exposure." *Trans. AIChE*, 31, 365-389.

Jesson, M. A., Bridgeman, J., and Sterling, M. (2015). "Novel software developments for the automated post-processing of high volumes of velocity time-series." *Adv. Eng. Softw.*, 89, 36-42.

Karpinska, A. M., and Bridgeman, J. (2016). "CFD-aided modelling of activated sludge systems – A critical review." *Wat. Res.*, 88, 861-879.

Karpinska, A. M., and Bridgeman, J. (2017). "Towards a robust CFD model for aeration tanks for sewage treatment – a lab-scale study." *Eng. Appl. Comp. Fluid* 11(1), 371-395.

Karpinska Portela, A. M. (2013). "New Design Tools for Activated Sludge Process."PhD thesis, Faculdade de Engenharia, Universidade do Porto, Portugal.

Larsen, P. (1977). "On the Hydraulics of Rectangular Settling Basins, Experimental and Theoretical Studies. Report No. 1001." Department of Water Resources Engineering. Lund Institute of Technology, University of Lund, Sweden.

Le Moullec, Y., Gentric, C., Potier, O., and Leclerc, J. P. (2010). "CFD simulation of the hydrodynamics and reactions in an activated sludge channel reactor of wastewater treatment." *Chem. Eng. Sci.*, 65(1), 492-498.

Levenspiel, O. (1999). *Chemical Reaction Engineering*, Wiley & Sons, New York, NY.

Menter, F. R. (1994). "Two-equation eddy-viscosity turbulence models for engineering applications." *AIAA J.*, 32(8), 1598-1605.

Mori, N., Suzuki, T., and Kakuno, S. (2007). "Noise of Acoustic Doppler Velocimeter Data in Bubbly Flows." *J. Eng. Mech.-ASCE*, 133(1), 122-125.

Mueller, J. A., Boyle, W. C., and Pöpel, H. J. (2002). *Aeration: principles and practice*, CRC Press, Boca Raton, FL.

Pereira, J. P., Karpinska, A., Gomes, P. J., Martins, A. A., Dias, M. M., Lopes, J. C. B., and Santos, R. J. (2012). "Activated Sludge Models Coupled to CFD Simulations." *Single and Two-Phase Flows in Chemical and Biomedical Engineering*, R. Dias, R. Lima, A. A. Martins, and T. M. Mata, eds., Bentham Science Publishers Ltd., 153-173.

Quasim, S. R. (1999). *Wastewater Treatment Plants: Planning, Design and Operation* CRC Press LLC, Boca Raton, FL.

Reardon, D. J. (1995). "Turning down the power." *Civil Eng.*, 65(8), 54-56.

Roache, P. J. (1998). "Verification of Codes and Calculations." *AIAA Journal*, 36(5), 696-702.

Samstag, R. W., Ducoste, J. J., Griborio, A., Nopens, I., Batstone, D. J., Wicks, J. D., Saunders, S., Wicklein, E. A., Kenny, G., and Laurent, J. (2016). "CFD for wastewater treatment: an overview." *Wat. Sci. Technol.*, 74(3), 549-579.

Samstag, R. W., and Wicklein, E. (2012). "Application of CFD to Activated Sludge Mixing Analysis. CFD Workshop- Presentation." *3rd IWA/WEF Wastewater Treatment Modelling Seminar-WWTmod2012* Mont-Sainte-Anne, QC.

Talvy, S., Cockx, A., and Line, A. (2007). "Modeling of oxygen mass transfer in a gas-liquid airlift reactor." *AIChE* 53(2), 316-326.

Tchobanoglous, G., Burton, F. L., Stensel, H. D., and Eddy, M. (2003). "Wastewater engineering: Treatment and reuse." *McGraw-Hill Series in Civil and Environmental Engineering*, McGraw-Hill New York, NY.

WEF (2009). "Energy Conservation in Water and Wastewater Treatment Facilities." *Water Environment Federation Manual of Practice No. 32*, McGraw-Hill, New York, NY.

Joint Task Force of the Water Pollution Control Federation and the American Society of Civil Engineers (WPCF-ASCE) (1988). "Aeration: A Wastewater Treatment Process." *WPCF- Manual of Practice No. FD-13. ASCE- Manuals and Reports on Engineering Practice No.68,* Water Pollution Control Federation, Alexandria, VA.

Yang, Y., Yang, J., Zuo, J., Li, Y., He, S., Yang, X., and Zhang, K. (2011). "Study on two operating conditions of a full-scale oxidation ditch for optimization of energy consumption and effluent quality by using CFD model." *Wat. Res.*, 45(11), 3439-3452.

Table 1. Aeration process design parameters.

	Air requirements ($m^3\ h^{-1}$)			
	AS plant	**Single tank**	**Z1**	**Z2**
Max. (1)	45819	3818	2279	1539
Average	31431	2619	1563	1056
Min.	20040	1670	997	673
Max. (2)	45819	3818	2864	955
Max. (3)	45819	3818	2279	1539

Note: 1 - actual operating parameters; 2 - optimization studies: airflow distribution between Z1 and Z2: 75 and 25%; 3 - optimization studies: total number of diffusers in Z1 and Z2: 2166.

Table 2. Characteristic features of several selected meshes.

Mesh No.	Min. cell size (m)	Max. face size (m)	No. of elements	Max. cell skewness	Notes
1	0.01	0.25	3846947	0.77	Converged solution (RAM/CPU expensive)
2	0.01	0.30	2223660	0.76	Converged solution
3	0.01	0.35	1266172	0.75	

Table 3. Physical properties of the phases enabled in CFD simulations of the aeration tank.

Phase	**Components**	**Physical properties**
Continuous	Water, tracer	ρ_L= 998.2 kg m^{-3} μ_L= 0.001 Pa s
	Activated sludge	ρ_L= 1450 kg m^{-3} (Larsen 1977) μ_L= 0.008 Pa s (Bokil and Bewtra 1972) Mass fraction – corresponds to the concentration* of 3.3 g L^{-1}
Dispersed	Air	ρ_G= 1.225 kg m^{-3} d_b= 0.5 ÷ 3.0 mm Mass fraction of oxygen: 0.23

Note: μ_L is dynamic viscosity of the fluid; *- average MLSS concentration measured in AS tank.

Table 4. Boundary and operating conditions set in CFD simulations of the aeration tank.

Place	Boundary Condition	Parameters/ Operating Conditions
Inlet pipe	Velocity inlet	v_L - corresponds to maximal and average operating flow rates I = 5 % D_h= 1.2 m α_G = 0 α_{tr} = 0 or α_{tr} = 1 (tracer injection time)
Outflow weir	Pressure outlet	I (backflow) = 5% D_h (backflow) = 0.4 m α_G (backflow) = 0
Diffusers	Velocity Inlet	v_G - corresponds to design and operating air flow rates in Z1 and Z2 (Table 1) I = 5% D_h = 0.16 m α_G = 1
Fluid surface	Degassing	p =101325 Pa
Side walls, bottom	No-slip wall	-
Fluid zone	-	T = 293 K ρ = 1.225 kg m^3

Note: I- turbulence intensity; D_h- hydraulic diameter; p, T and ρ- operating pressure, temperature and density; α_{tr}- volume fraction of tracer.

Table 5. Hydrodynamic and oxygen transfer parameters obtained from the CFD simulations of the aeration tank for different operating scenarios.

Operating scenario	$v_{L,hor}$	v_L		v_a		α_G		ε		$k_L a_{20}$		$\alpha k_L a_{20}$		**DO***	
	m s^{-1}					%		$\times 10^{-3}$ m^2 s^{-3}		d^{-1}		d^{-1}		mg L^{-1}	
	Tank	Z1	Z2	Z1	Z2	Z1	Z2	Z1	Z2	Z1	Z2	Z1	Z2	Z1	Z2
1	0.22	0.27	0.24	0.30	0.33	0.43	0.34	1.62	1.00	186	130	56	104	10.05	10.28
2	0.23	0.25	0.24	0.30	0.31	0.56	0.16	1.20	0.36	224	46	67	37	10.09	10.24
3	0.11	0.17	0.08	0.25	0.21	0.49	0.31	0.58	0.34	161	90	48	72	10.06	10.28

Note: 1 - original diffuser layout & operating scenario; 2 - original diffuser layout & modified operating scenario; 3 - modified diffuser layout & original operating scenario, *** -** equilibrium concentration reached at the oxygenation time of 15 min.

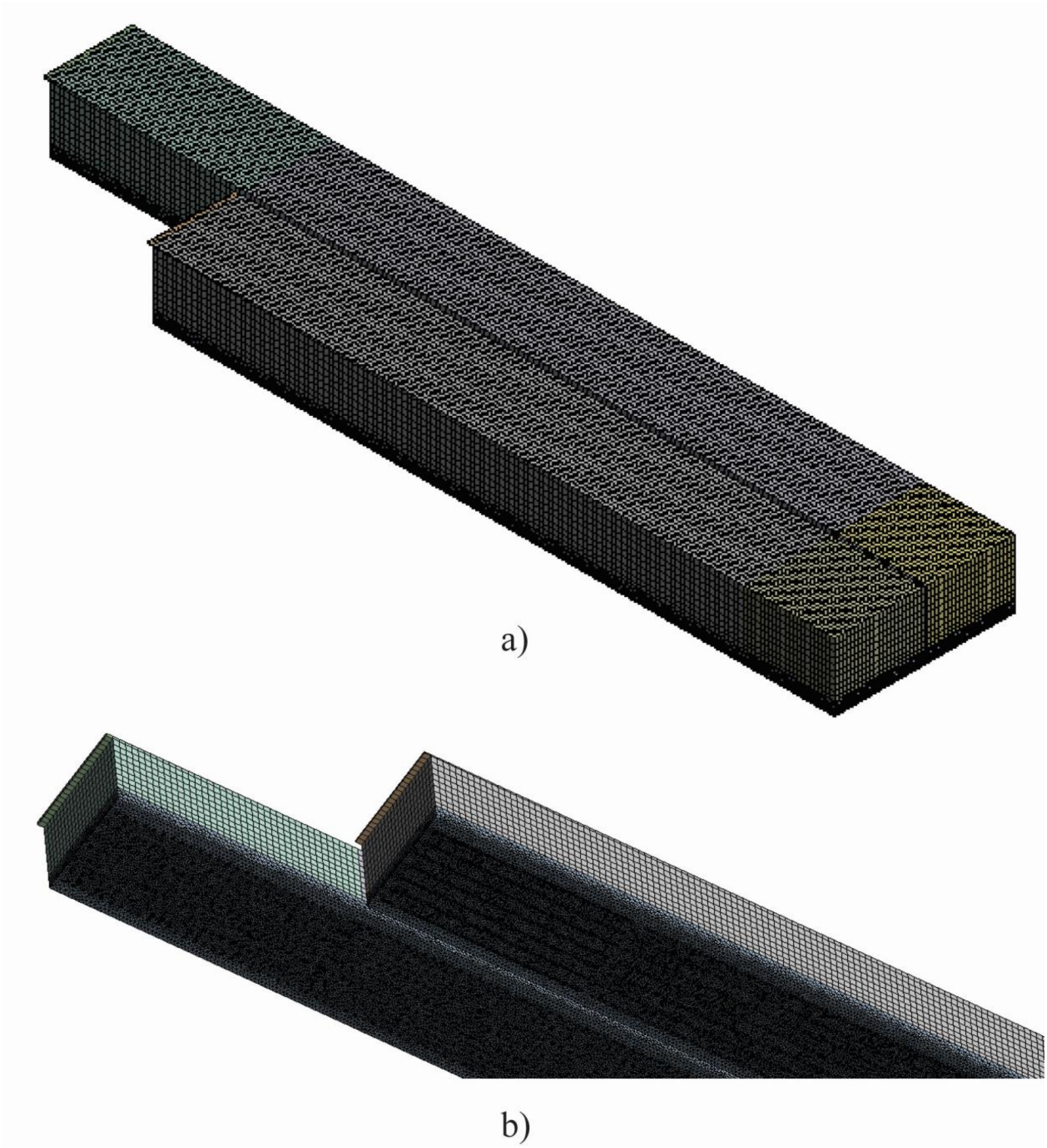

Fig. S1. Computational mesh a) iso-view; b) detail – mesh refinement in the diffuser region (bottom).

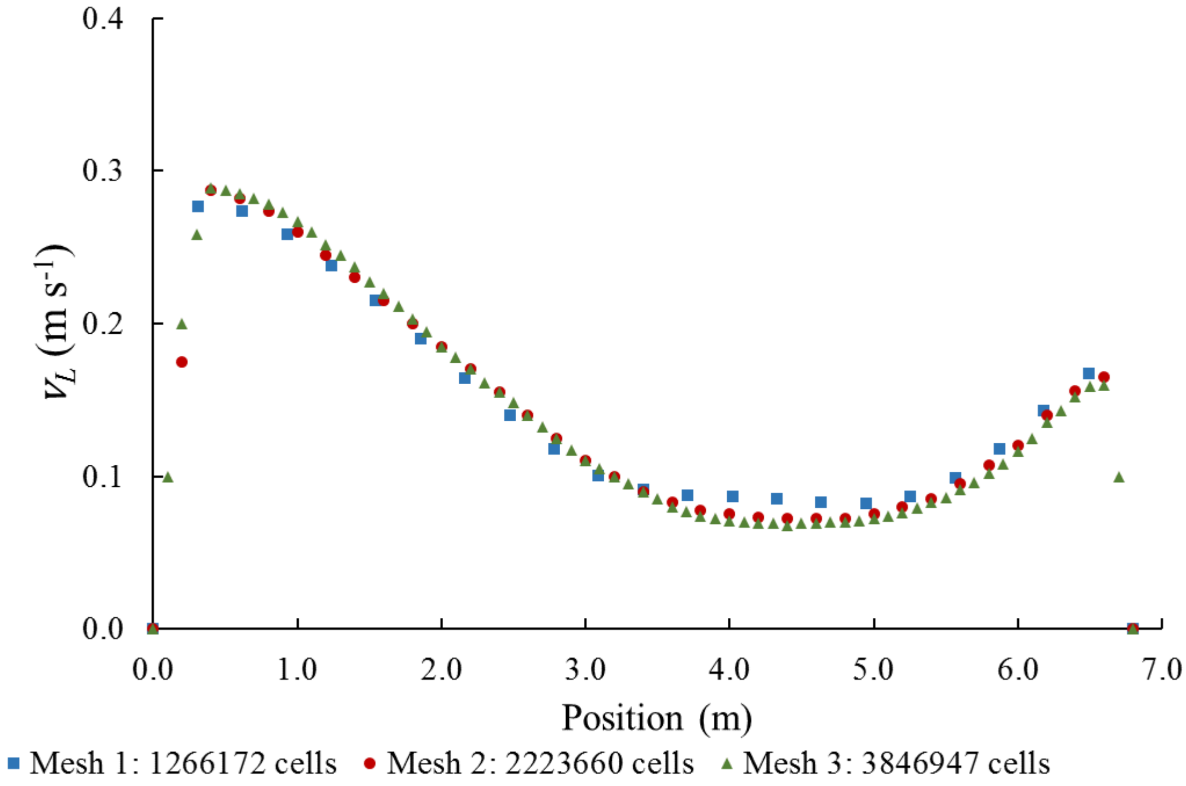

Fig. S2. Average liquid phase velocity on a transversal line across the aeration tank (Z1, L= 30 m, H= 4.9 m) obtained with different mesh sizes.

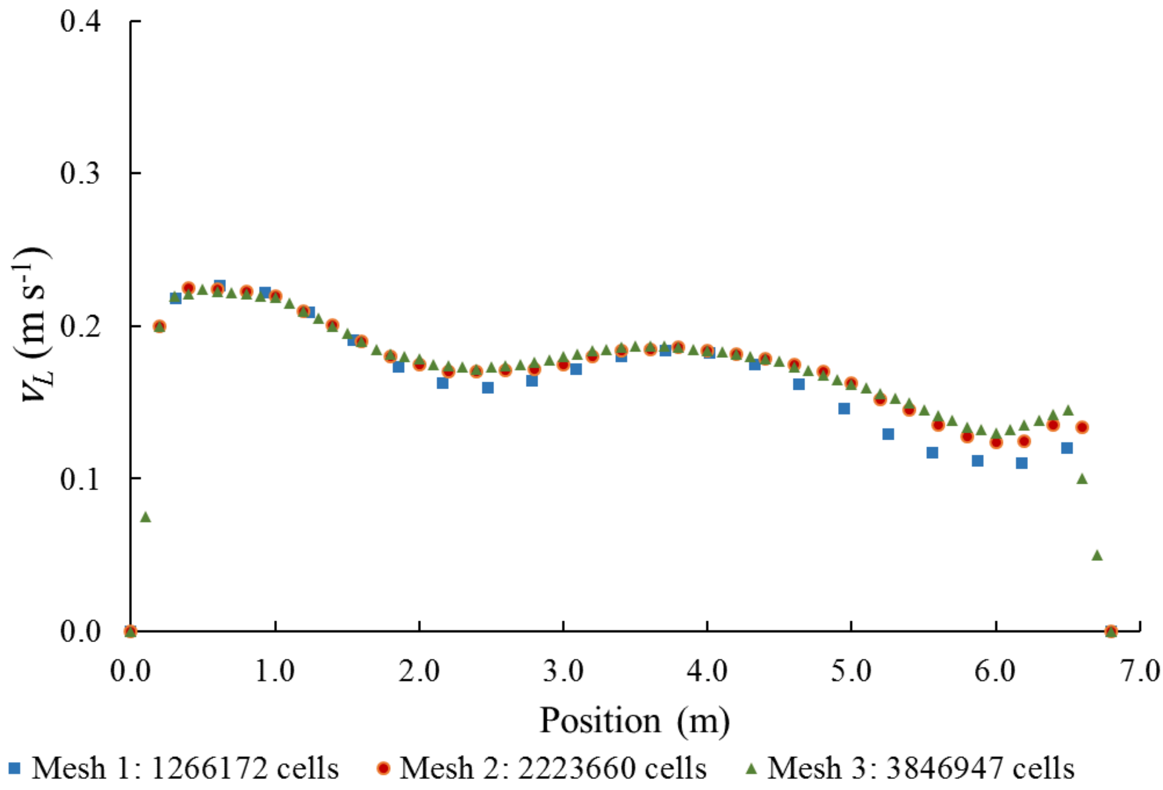

Fig. S3. Average liquid phase velocity on a transversal line across the aeration tank (Z1, L= 30 m, H= 4.5 m) obtained with different mesh sizes.

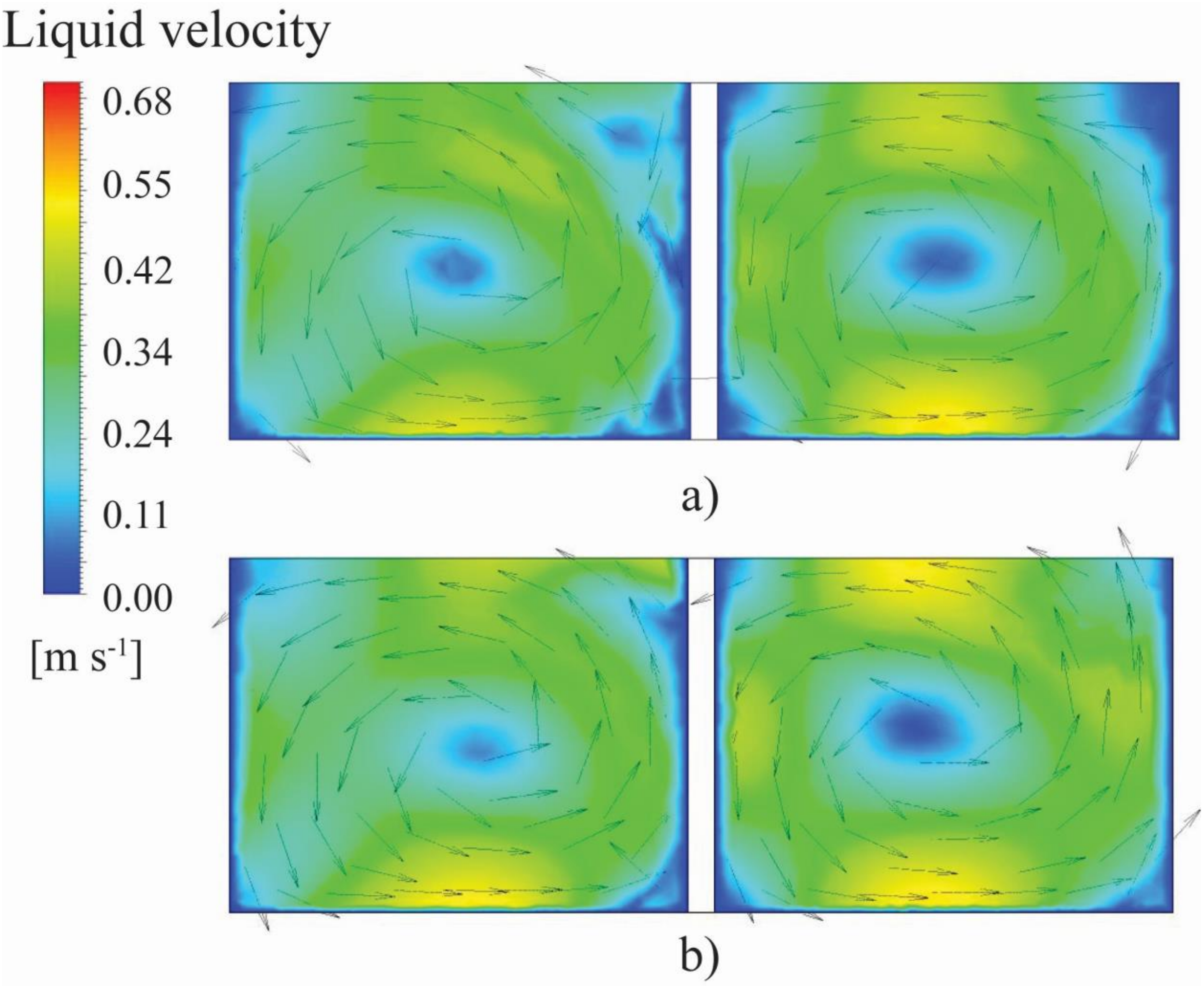

Fig. S4. Contour and vector maps of the velocity magnitude obtained for Q_L = 0.1 m^3 s^{-1}, Q_a = 1.1 m^3 s^{-1} with a) neutral density approach, and b) accounting for the presence of sludge (L =30 m).

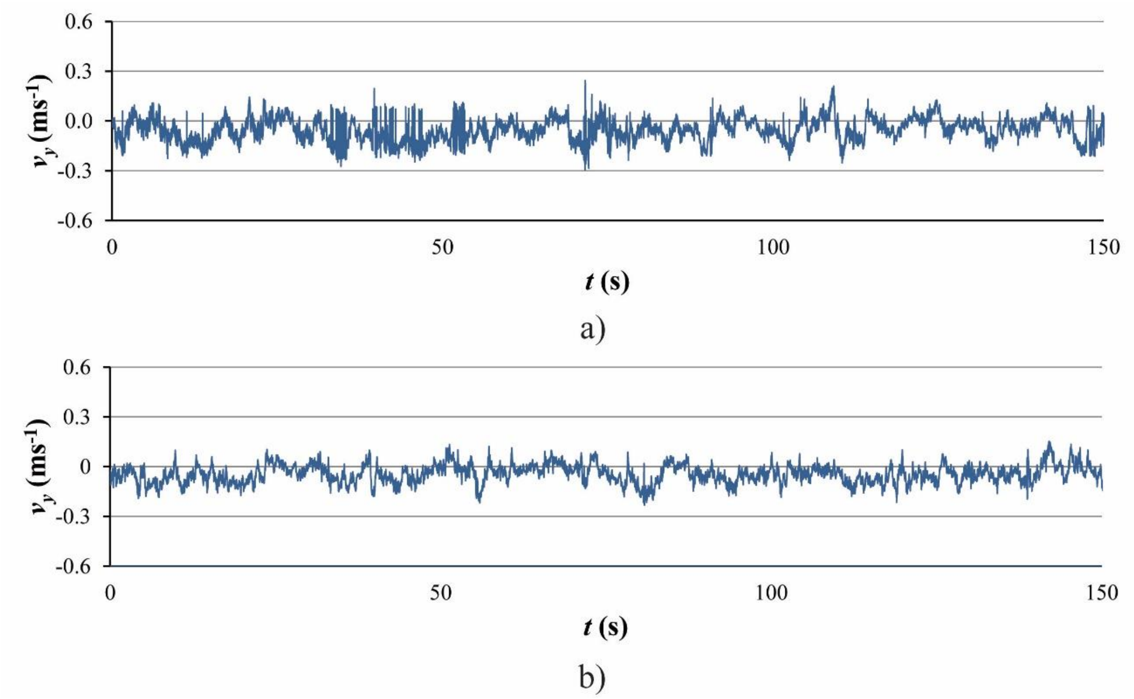

Fig. S5. ADV time-series obtained in the measurements of the vertical component of the water velocity in the full-scale AS tank: a) raw data-set; b) clean data-set after despiking procedure.

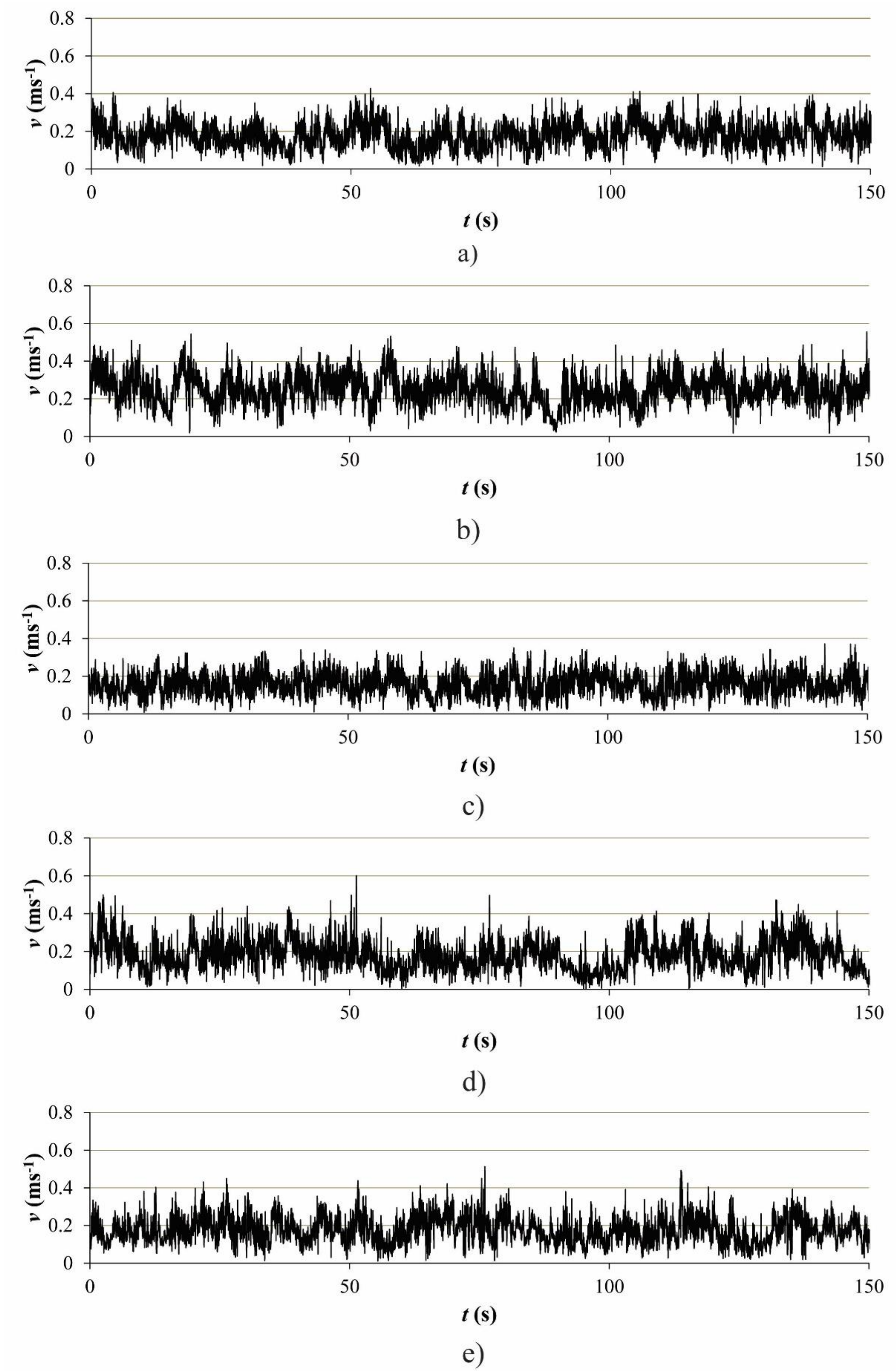

Fig. S6. The filtered ADV time-series obtained in the measurements of the water velocity in the full-scale aeration tank at the submergence of 0.3 m and at the distance of: a) 0.4 m; b) 1.85 m; c) 3.30 m; d) 4.80 m; e) 6.25 m from the external wall.

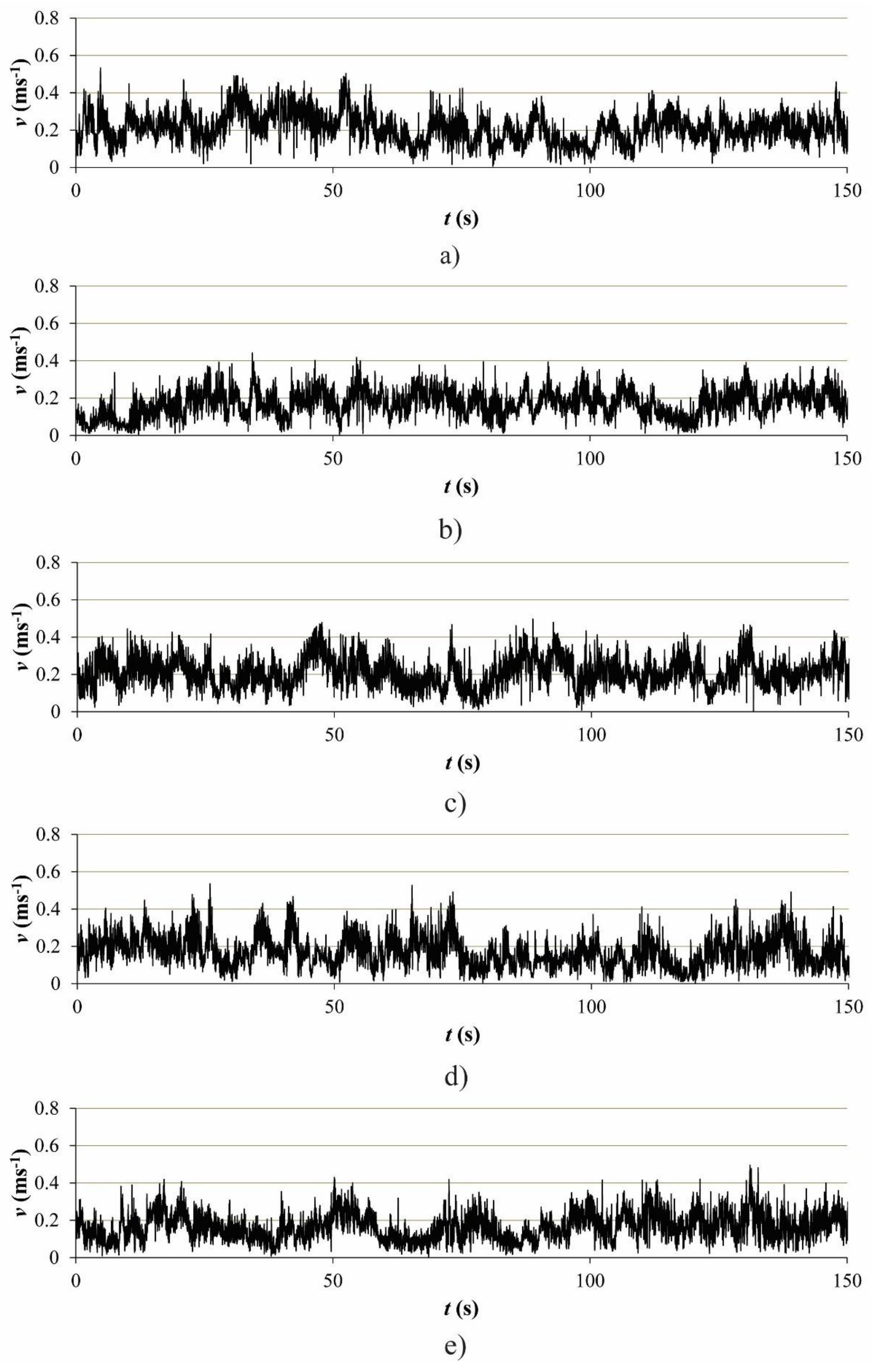

Fig. S7. The filtered ADV time-series obtained in the measurements of the water velocity in the full-scale aeration tank at the submergence of 0.7 m and the distance of: a) 0.4 m; b) 1.85 m; c) 3.30 m; d) 4.80 m; e) 6.25 m from the external wall.

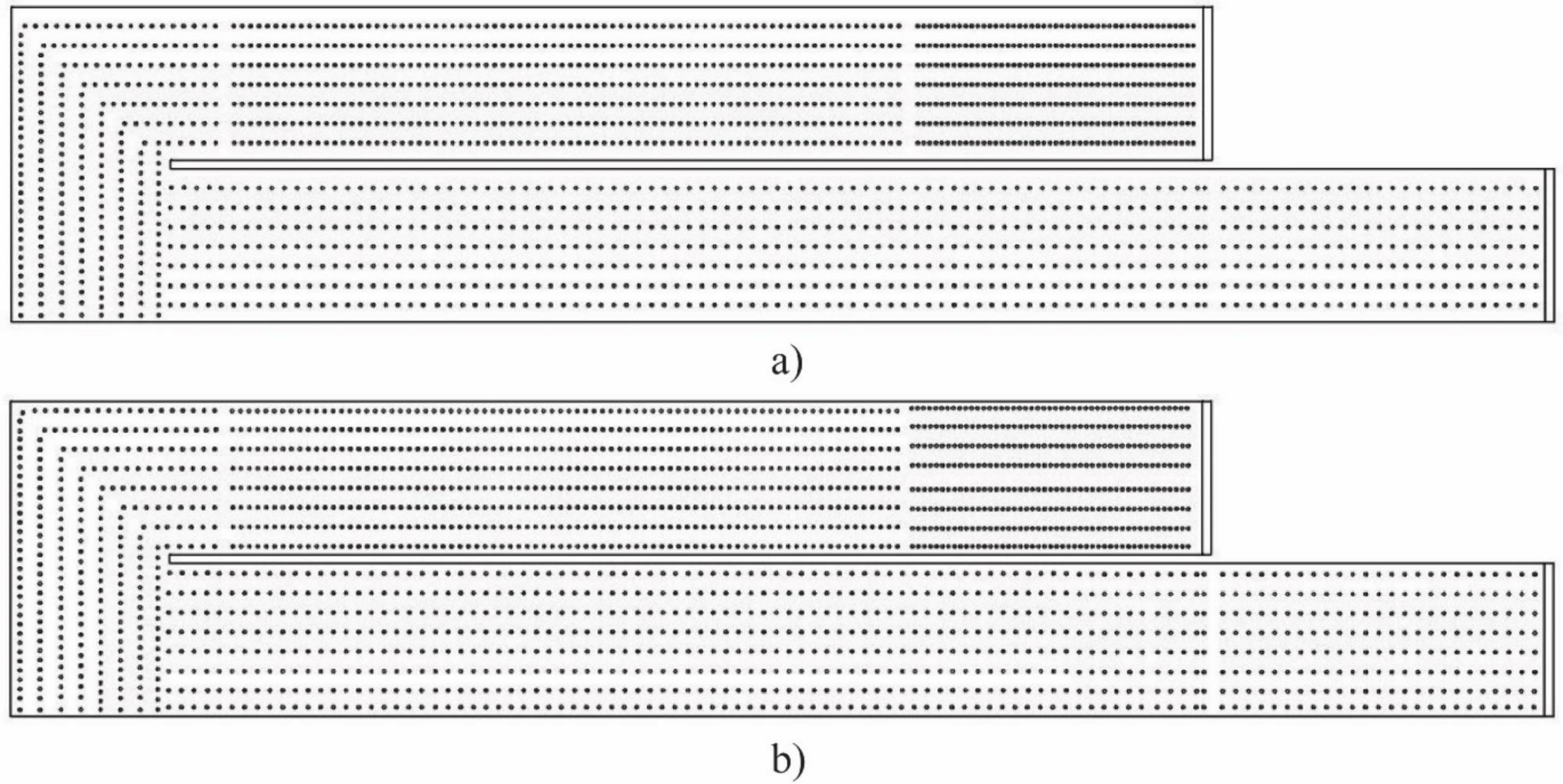

Fig. S8. Diffuser grid a) original layout; b) modified layout (one diffuser added to each row).

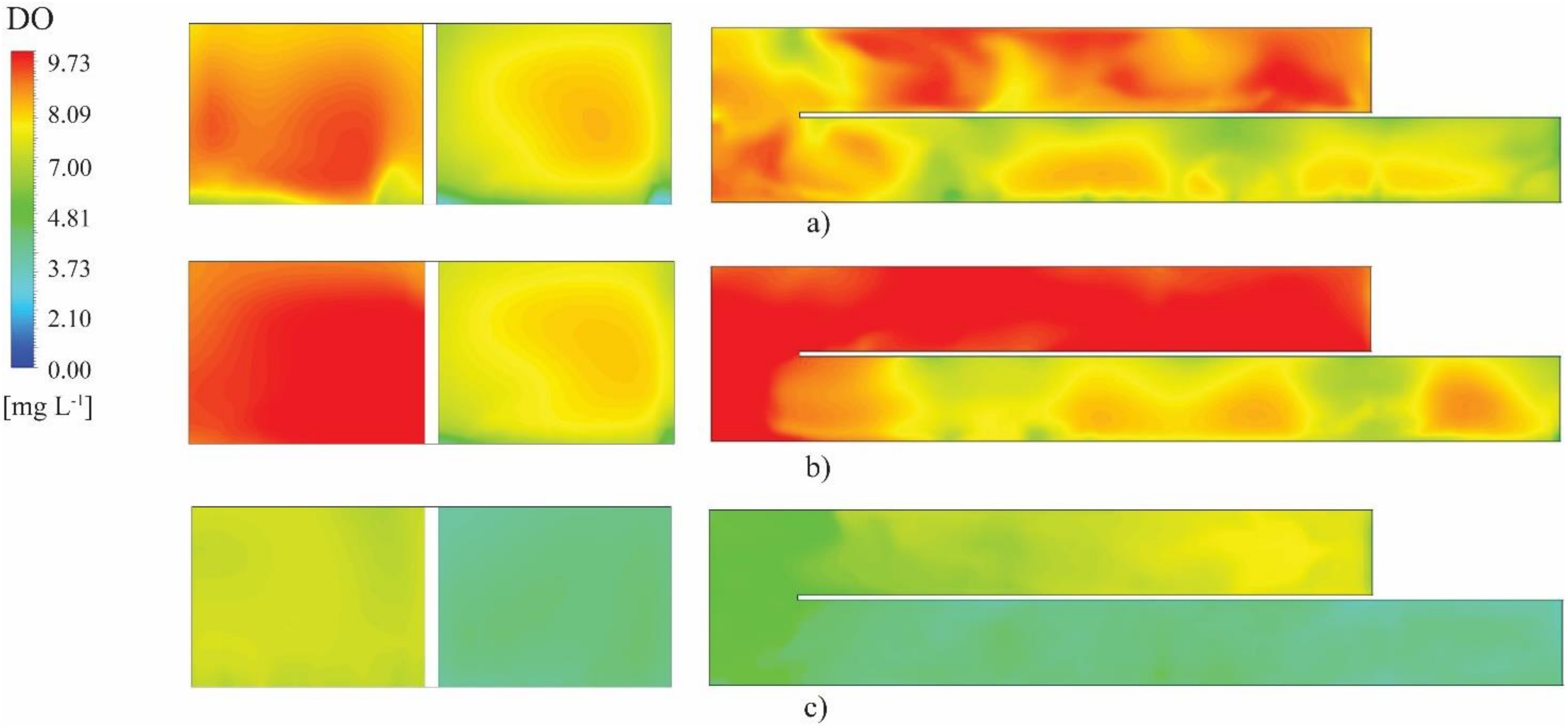

Fig. S9. Evolution of the DO concentration in the AS tank after aeration time of 2 mins for a) original diffuser layout & operating scenario; b) original diffuser layout & modified operating scenario; c) modified diffuser layout & original operating scenario.